Sound produced by the rapidly inflating Santiaguito lava dome, Guatemala

Jeffrey B. Johnson[1] and Jonathan M. Lees[2]

Received 14 September 2010; revised 24 September 2010; accepted 30 September 2010; published 20 November 2010.

[1] Vertical inflation of the Caliente lava dome at Santiaguito (Guatemala) occurs coincidentally with the onset of explosive eruptions and produces infrasound that is generally peaked between 0.5 and 2 Hz with amplitude of up to 5 Pa (at ~1 km from vent). Inflation of up to ~1 m progresses rapidly (within ~2 s) and can encompass the entire surface of the ~200-m-diameter dome. We use particle image velocimetry to quantify the time history of dome uplift and demonstrate that deflection of a volcano's solid surface can generate infrasound waves with amplitudes of a few Pa. The volumetric displacement history is used to model linear volumetric acoustic sources, both compact and of finite extent. Synthetic waveforms match recorded infrasound in terms of timing and frequency content. Amplitude fit is very good for a station located 3.3 km from the vent and less good for stations shielded by near vent topography. **Citation:** Johnson, J. B., and J. M. Lees (2010), Sound produced by the rapidly inflating Santiaguito lava dome, Guatemala, *Geophys. Res. Lett.*, *37*, L22305, doi:10.1029/2010GL045217.

1. Introduction

[2] Volcanoes generate intense sounds in the infrasound band (below 20 Hz) with peak amplitudes often at periods/frequencies of a few seconds to a few Hertz [*Johnson et al.*, 2004]. Typical Strombolian activity can produce excess pressures up to hundreds of Pa recorded within a few kilometers of a vent, for example at Erebus [*Rowe et al.*, 2000] and Fuego [*Lyons et al.*, 2010]. Vulcanian and ash-rich eruptions are also able to produced sound pressure levels that, when reduced to a kilometer, are often in excess of tens of Pa, for example at Arenal [*Hagerty et al.*, 2000], Tunugurahua [*Ruiz et al.*, 2005], and Sakurajima [*Yokoo et al.*, 2009]. Volcanoes with persistently open vents are also able to emit high intensity infrasound of a few to tens of Pa at 1 km, which is often present even without a flux of pyroclastic material, for example at Etna [*Ripepe et al.*, 2001], Stromboli [*Marchetti et al.*, 2009], Kilauea [*Fee et al.*, 2010], and Villarrica [*Johnson et al.*, 2004].

[3] The duration, frequency content, and envelope of an infrasound waveform provide insight into the style of a volcanic eruption. Often an eruptive event will begin with a high-amplitude compression followed by a distinct rarefaction manifesting an N-shaped pulse [e.g., *Morrissey and Chouet*, 1997; *Johnson et al.*, 2004]. Such signals correspond to an outward acceleration of atmosphere followed by a deceleration and are predicted for a variety of linear acoustic sources, such as idealized balloon bursts [*Deihl and Carlson*, 1968], or for shock waves, which begin as discontinuous pressure records that decay into acoustic waves [*Kinney and Graham*, 1985]. Volcano N-shaped waves may arise from sources as varied as subsonic distension of a solid free surface (as demonstrated here), movement of a fluid free surface, or supersonic emission of gas and pyroclasts.

[4] Coincident visual and infrasound observations of volcanic activity provide a powerful tool for distinguishing between various sound excitation mechanisms. At Erebus and Erta Ale lava lakes, for instance, infrasound is seen to result both from the distension of the lava lake (as large bubble slugs reach the surface) followed by rupturing and explosion of pressurized gases [*Rowe et al.*, 2000; *Bouche et al.*, 2010]. At Santiaguito, high-resolution video reveals rapid inflation of the solid surface of the active dome that is coincident with (or immediately precedes) the onset of gas emissions. As at Erebus, both processes produce detectable infrasound. This paper focuses on the rapid inflation of the solid Santiaguito dome surface and its relation to the N-shaped infrasound pulse onset. Previous study by *Yokoo et al.* [2009] attributed pre-eruption lava plug swelling at Sakurajima to a weak infrasound compression that led, within a fraction of a second, to the primary eruption event. In this study we provide time-synced video evidence to support uplift of the solid dome as the source of the initial infrasound compression.

2. PIV Analysis

[5] To quantify dome uplift using video cameras we perform a particle image velocimetry (PIV) analysis on still images extracted from high definition (1800 × 1080 pixels) 30 fps video [*Johnson et al.*, 2008]. Video was filmed with Casio EX-F1 cameras situated near the Santa Maria summit (SG1; 3660 m) and on the south ridge of Santa Maria (SG2; 3460 m). Both were trained with their full optical zoom on the summit region of the Caliente vent (Figure 1). For SG1 the targeted dome was ~2700 m from Santa Maria at an azimuth of 225° and an inclination angle of 25° below the horizontal. The horizontal field of view at the dome was ~225 m corresponding to about 12.5 cm per pixel. Line resolution at the distance of the dome was also 12.5 cm/pixel, or 30 cm/pixel when projected on to a horizontal plane (approximating the surface of Caliente) and 13.5 cm/pixel when projected on to the vertical. Camera footage was time-synchronized to 1/30 s using hand-held GPS units.

[6] In the PIV analysis we divide comparison images into 2/3 overlapping 100 × 100 pixel grid nodes (12.5 m × 30 m horizontal projections) and then assess relative movement in each grid node using a 2D image cross correlation (see

[1]Department of Earth and Environmental Science, New Mexico Institute of Mining and Technology, Socorro, New Mexico, USA.
[2]Department of Geological Sciences, University of North Carolina, Chapel Hill, North Carolina, USA.

0094-8276/10/2010GL045217

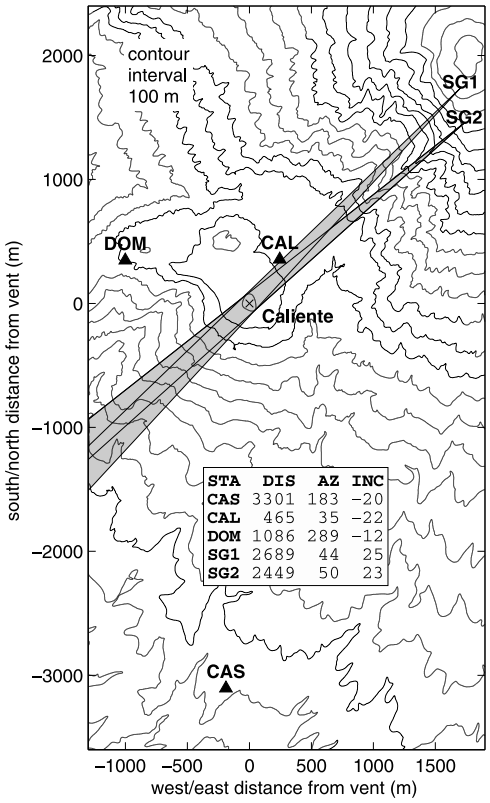

Figure 1. Map of Santiaguito domes showing active Caliente vent and Santa Maria summit with indicated field of views for cameras SG1 and SG2. Infrasound stations CAS, CAL, and DOM are indicated along with their distances (in m), azimuth, and inclination from horizontal (in degrees) from vent.

Figure 2 and Animations 1 and 2 of the auxiliary material). PIV is performed on 764 grid nodes distributed over the 200-m-diameter vent region. Starting with a control image 1 s prior to the pyroclastic emissions we calculate correlated movement for successive image frames until normalized cross-correlation values drop below 0.8. Relative motion of the dome surface is determined in single pixel increments, which project to 13.5 cm in the vertical. Because cross-correlation is calculated to the nearest integer pixel (and results in a stair-step displacement record) we smooth the time series of grid node movement using a low-pass 7 Hz two-pole Butterworth filter, which also helps to reduce optical noise due to refraction and/or camera shake.

[7] Image cross correlation values drop below 0.8 when gas emissions block the view to the surface of the dome within the grid node field of view. At this point we are unable to track continued dome surface movement, however it is notable dome inflation has generally slowed by the time the dome surface becomes hidden. In some grid nodes there is a suggestion of slight dome deflation before the surface is obscured. In other places, notably around the periphery of the inflating pad, PIV appears to show dome deflation coincident with the onset of degassing and inflation elsewhere (see left side of Figures 2a and 2b).

[8] In the PIV study of Santiaguito dome by *Johnson et al.* [2008] a single camera was used and primary motion was assumed to be vertical. Image analyses from dual cameras deployed in January 2009 confirm that surface motion vectors are predominantly vertical from each camera perspective. PIV-inferred uplift history is projected in the vertical direction and compared for two different events in Figure 3.

3. Dome Inflation and the Seismoacoustic Wavefield

[9] *Johnson et al.* [2008] used particle image velocimetry (PIV) to quantify the rapid uplift of the Caliente dome surface and relate it to broadband seismic records. They found that the amount of uplift scaled well with the long period (LP) band seismic displacement for a suite of eruptive events. They inferred that the volcanic edifice responds seismically to the upward momentum change of the rapidly uplifting lava dome. Modeling the volcano response as a downward-directed single vertical force they matched observed displacement seismograms with a dome of 20–80 m uniform thickness.

[10] In addition to generating LP seismicity, the rapid dome uplift also displaces tens of thousands of cubic meters of overlying atmosphere producing infrasound. Eruption infrasound from Santiaguito often begins with an N-shaped pulse consisting of a compression followed by rarefaction (lasting 1–2 s) and with peak-to-peak pressures of 1–5 Pa (at distances of about 1 km). For the 96 events recorded in January 2009 infrasound frequency spectra was peaked between 0.5 to 1.5 Hz with only 2–3% of the infrasound power occurring at frequencies greater than 7 Hz. Coincident with, or shortly following, the initial N-shaped pulse an infrasound tremor-like coda persisted for tens of seconds to several minutes and corresponded to the duration of observable gas emissions, which also has a characteristic contribution to the infrasound wavefield [*Jones and Johnson*, 2010].

[11] As with the initial seismic LP response, the timing of the acoustic arrival corresponds well to the onset of dome uplift and the amplitude of the pulse appears to scale well with the magnitude of dome uplift. These observations encouraged us to model the recorded infrasound as a response to dome uplift behaving like a speaker diaphragm.

[12] For a baffled speaker, with source radius that is small compared to the radiated sound wavelengths, the source may be approximated as compact [*Dowling*, 1998], and the recorded pressure field $p(t)$ is proportional to the momentum change of the atmosphere:

$$p(t) = \frac{1}{\Omega r}\frac{d^2M(t - r/c)}{dt^2} \quad (1)$$

where d^2M/dt^2 is the acceleration history of mass injected at the point source, $t - r/c$ is the retardation time at a specific station, with distance r and for sound propagating with a speed c. The constant Ω is a solid angle accounting for sound spreading into a whole space (4π), half space (2π), or the subtended atmosphere above an idealized stratovolcano cone with 30° slope (3π).

[13] PIV is used to quantify the dome uplift and associated atmospheric displacement history, which can be converted to an atmospheric volume acceleration. Mass history $M(t)$ is calculated from the PIV-inferred volume displacement history of the atmosphere and an estimated atmospheric density (approximated here at 1 kg/m^3 for the ~2500 m elevation of

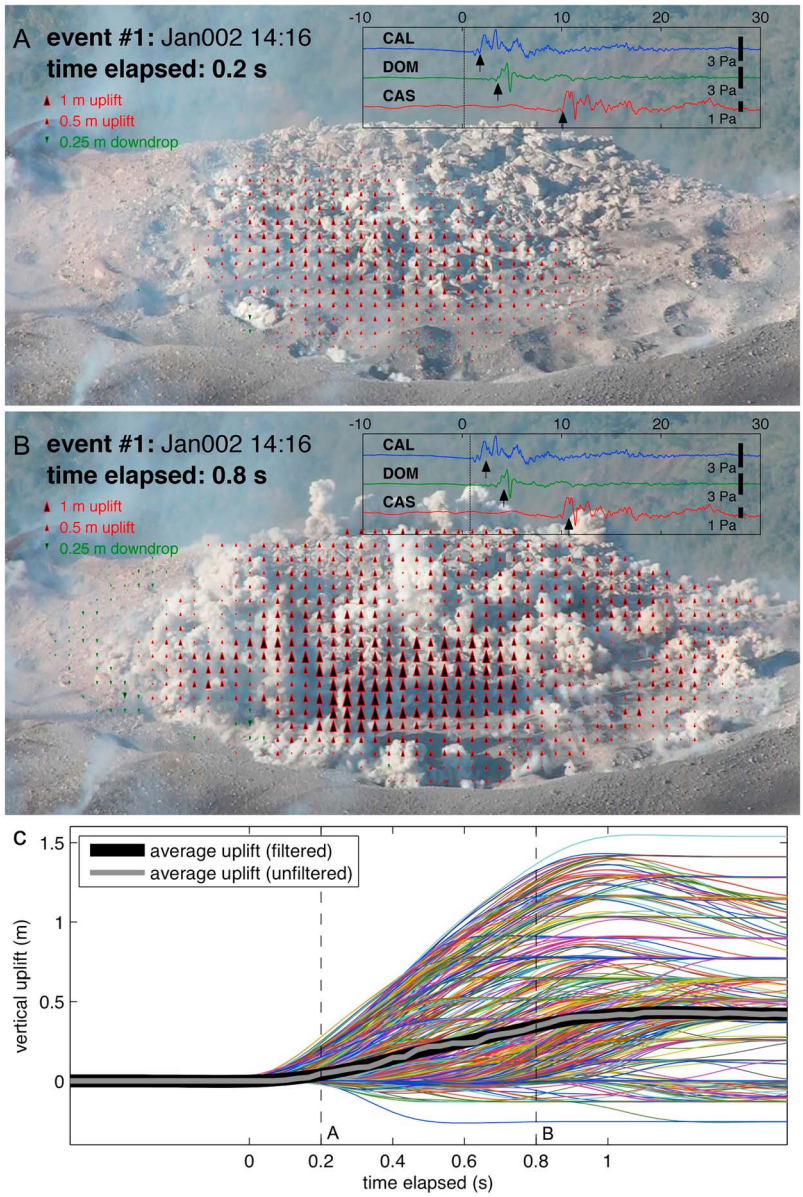

Figure 2. (a and b) Example PIV dome uplift for an event as seen by camera SG1. Vectors indicate vertically projected dome surface motion. Red and green correspond to uplift and down-drop (respectively) along with vertical motion scale bars and frame times. (c) Smoothed time history of uplift is plotted for 774 independent grid nodes and averaged across the 31,000 m^2 dome surface (black). Animated PIV sequences for the two featured events are provided in the auxiliary materials.

the Caliente vent). Under the assumption of a compact acoustic piston-type motion, in which the source region is small compared to the characteristic emtitted sound wavelength, the volume flux, and synthesized acoustic wavefield can be calculated from the integrated upward volume acceleration of the dome (Figures 3c and 3d). It is noteworthy that for certain events the inferred volume flux shows dual peaks (e.g., at ~0.25 and ~0.8 s in Figure 3c), which causes the modeled acoustic pulse (Figure 3d) to deviate from an ideal N-shaped signal. We consider that the dip in flux (between the two peaks) is likely due to PIV tracking issues as gas is erupted and begins to obscure the dome region.

[14] At Caliente, uplift occurs over a 200-m-diameter plateau, which has about the same approximate dimension as a 1.7 Hz acoustic wavelength (e.g., $c = 340$ m/s). Considering the potentially non-compact nature of this acoustic source, we also synthesize the acoustic wavefield as a superposition of discrete volumetric sources consisting of acoustic monopoles distributed over a horizontal surface [e.g., *Dowling*, 1998]. PIV-inferred movements from each of the N grid nodes can be used to synthesize an infrasound waveform according to

$$p(t) \sum_{n=1}^{N} \frac{1}{\Omega r(i,j)} \frac{d^2 M_{i,j}(t - r(i,j)/c)}{dt^2} \quad (2)$$

where retardation times are calculated independently for each node using variable distances $r(i,j)$ to a particular station. The time history of mass displacement of the atmosphere at a

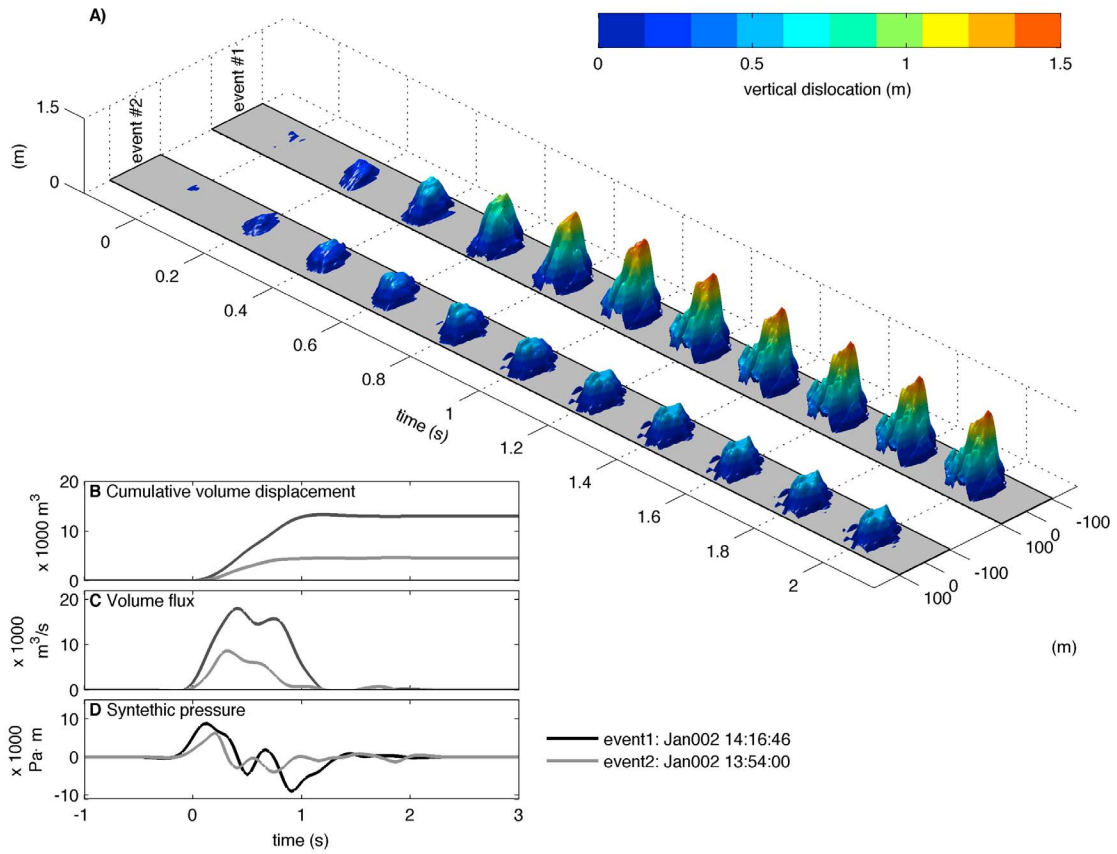

Figure 3. (a) Comparison of dome uplift for two featured events occurring on 02 January 2009 as seen with PIV. Video of the dome distension, along with mapped PIV vectors and time-synchronized infrasound waveforms, is provided in the auxiliary materials. (b) Volume displacement, (c) time derivative of volume displacement, and (d) second time derivative of volume displacement converted to a synthetic excess pressure time series (assuming a compact source).

given node, $M_{i,j}$, equals the product of the grid node area, vertical uplift, and density of the displaced atmosphere.

4. Validation of Dome Inflation Model of Sound Production

[15] Both compact sources and finite-element source distributions are used to synthesize infrasound waveforms for stations deployed during January 2009 (Figure 4). In part because the PIV motion is low-pass filtered (<7 Hz), the two modeling methods produce similarly-shaped infrasound pulses. Only a small reduction in modeled peak-to-peak amplitudes (7–55%; see Figures 4a–4f) is seen for the distributed source region due to destructive interference. This signal diminution is slight because the dome uplift source excitation mechanism is relatively slow, resulting in a predominance of low frequency energy around 0.6 to 0.9 Hz producing long wavelength sound that is largely coherent across the 200-m-diameter dome.

[16] Timing and shape of the synthetic infrasound pulses and observed infrasound waveforms are generally in good agreement (Figure 4). The concussion modeled by the PIV-inferred uplift is propagated across the network at 343 m/s (sound speed at 20°C) and its arrival coincides with the first significant infrasound compression recorded across the sensor network. The shape of the synthetic waveforms also matches the first significant infrasound pulse, especially for stations DOM and CAS. Compression and rarefaction endure for about and 1.5 and 1.2 s, for events #1 and #2 respectively and synthesized infrasound frequency spectra match the recorded infrasound spectra (Figure 4).

[17] Synthetic infrasound amplitude fit is excellent for station CAS (3.3 km from the vent) and relatively poor for the closest station CAL (at ~0.5 km). A misfit is expected considering that the recorded sound amplitudes at CAS are generally only 70–80% of the signal amplitude at CAL, despite CAS's location ~8 times further away. We suspect that CAL receives unexpectedly low signal because the dome topography acts as a barrier to incident acoustic energy. Sound energy must diffract along the topographic rim of Caliente Dome in order to reach CAL (and to a lesser extent DOM). Our observation that infrasound pressures recorded in the vicinity of Santiaguito do not obey a $1/r$ amplitude decay bring into question the reliability of using a single infrasound station to quantify a volcano's acoustic source strength or total radiated power [e.g., *Johnson et al.*, 2004; *Firstov and Kravchenko*, 1996]. Further study of infrasound station site response related to mountain topography is warranted.

5. Discussion: On the Source of Infrasound at Santiaguito

[18] The first impulse of the recorded Santiaguito infrasound wave train agrees well with the predicted timing,

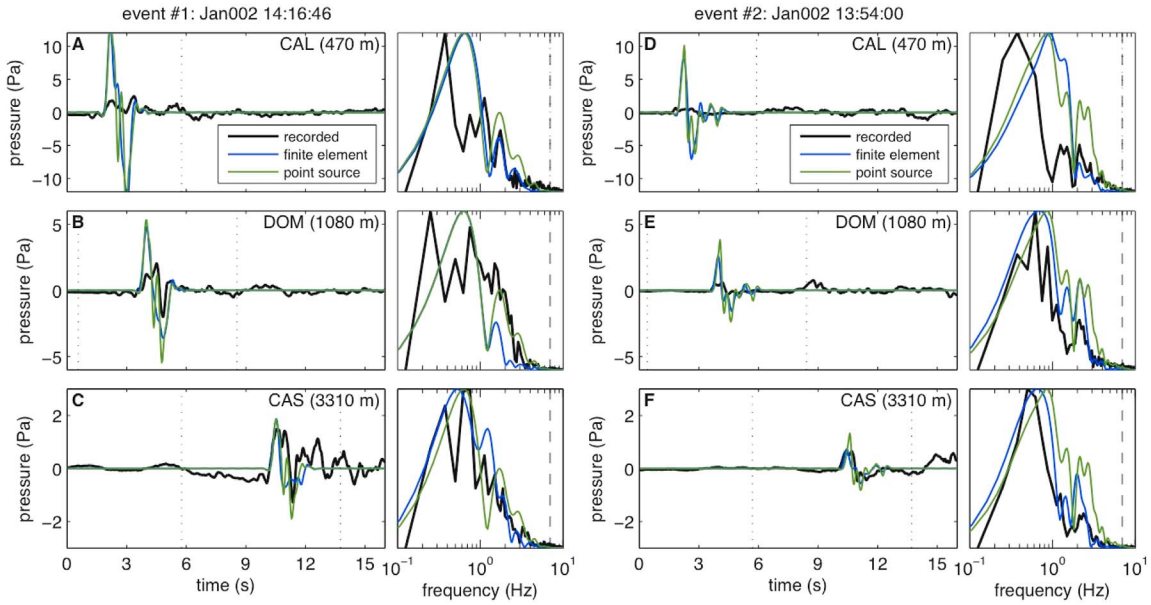

G peak-to-peak amplitudes

		Event #1: 14:16			*Event #2: 13:54*		
		p_{CAL}	p_{DOM}	p_{CAS}	p_{CAL}	p_{DOM}	p_{CAS}
i	synthetic (compact source)	24.7	10.8	3.6	14.2	6.2	2.1
ii	synthetic (finite source)	22.7	8.5	2.5	13.3	4.2	1.3
iii	Ratio (i/ii)	1.08	1.28	1.44	1.07	1.48	1.55
iv	Recorded pressure	3.6	4.0	2.8	1.9	1.3	1.4
v	Ratio (iv/ii)	0.16	0.47	1.11	0.14	0.30	1.05

Figure 4. (a–f) Modeled waveforms and corresponding frequency spectra (blue and green lines) plotted against filtered (0.05 to 7 Hz) signals (black) at three different stations. Normalized amplitude spectra is calculated for 8-s windows (denoted by dashed lines in time series). (g) Comparative table of synthetic and recorded peak-to-peak infrasound amplitudes.

amplitude, and general shape of the sound associated with rapid uplift of the solid dome surface. Notably, the amplitude of the infrasound associated with dome uplift (<5 Pa at distances of 1 km) contrasts with the generally much-higher peak infrasound amplitudes recorded at many other exploding volcanoes worldwide, e.g., see summary list of *Johnson et al.* [2004]. Following the initial dome uplift pulse, the Santiaguito infrasound wave train is comprised of pulses and low amplitude (few Pa) tremor that endure for tens of seconds to tens of minutes. The wave train coda is visually associated with explosive emissions of pyroclastics and gas and structure of the coda can sometimes be correlated with individual explosive bursts [*Jones and Johnson*, 2010]. In general, the low infrasound amplitude of the Santiaguito explosion signals can be attributed to low volume accelerations because upward growth of the eruption column is driven largely by buoyant rise [*Yamamoto et al.*, 2008].

[19] From recorded infrasound records it is apparent that the Santiaguito eruption style differs from the Vulcanian eruptions recorded at Sakurajima. Although both volcanoes commence with dome inflation or inferred swell of a lava plug, Sakurajima produced high amplitude (>100 Pa at a few km) infrasound blast waves less than a second following the movement of the lava plug [*Yokoo et al.*, 2009]. Notably the infrasound associated with lava plug swell at Sakurajima was similarly weak (1–3 Pa) compared to Santiaguito dome uplift infrasound. This demonstrates that volume accelerations of a solid free surface can often produce detectable sounds, but are often far smaller than volume accelerations associated with an explosively expanding gas cloud.

6. Conclusion

[20] Infrasound recorded local to a volcano, as part of arrays or networks, can reveal deviations from expected radial fall-off that might be predicted for spherical spreading in a homogenous atmosphere without obstructing topography. Recorded infrasound signals, which are not attributed to propagation or site effects, can then be used to infer source dimensions, material flux, and eruption style. Volcano acoustic signals generally reflect accelerations of solid or fluid materials at the free surface. In the case of Santiaguito, acoustic waves are initially produced by uplift of a solid free surface and this signal is both coincident with, and followed by, vigorous degassing, which is likely responsible for much of the infrasound coda. In general, understanding

the extent to which free surface motions, including solid-atmosphere, fluid magma-atmosphere, and erupted gas-atmosphere, can ensonify the atmosphere is vital for advancing infrasound's contribution to multi-disciplinary volcano geophysical field study.

[21] **Acknowledgments.** We appreciate field assistance from G. Waite, J. Lyons, R. Wolf, R. Sanderson, J. Anderson, A. Miller, and personnel from INSIVUMEH (Guatemala). Support was provided by NSF EAR grants 0738802, 0838562, and the National Geographic Society Expeditions Council.

References

Bouche, E., S. Vergniolle, T. Staudacher, A. Nercessian, J.-C. Delmont, M. Forneux, F. Cartault, and A. Le Pichon (2010), The role of large bubbles detected from acoustic measurments on the dynamics of Erta 'Ale lava lake (Ethiopia), *Earth Planet. Sci. Lett.*, *295*, 37–48, doi:10.1016/j.epsl.2010.03.020.

Deihl, D. T., and F. R. Carlson (1968), "N Waves" from bursting balloons, *Am. J. Phys.*, *36*(5), 441–444, doi:10.1119/1.1974556.

Dowling, A. P. (1998), Steady-state radiation from sources, in *Handbook of Acoustics*, edited by M. Crocker, pp. 99–117, John Wiley, New York.

Fee, D.,M. Garces, M. Patrick, B. Chouet, P. B. Dawson, and D. Swanson (2010), Infrasonic harmonic tremor and degassing bursts from Halemaumau Crater, Kilauea Volcano, Hawaii, *J. Geophys. Res.*, doi:10.1029/2010JB007642, in press.

Hagerty, M. T., M. Protti, S. Y. Schwartz, and M. A. Garces (2000), Analysis of seismic and acoustic observations at Arenal Volcano, Costa Rica, 1995–1997, *J. Volcanol. Geotherm. Res.*, *101*(1–2), 27–65, doi:10.1016/S0377-0273(00)00162-1.

Johnson, J. B., R. C. Aster, and P. R. Kyle (2004), Volcanic eruptions observed with infrasound, *Geophys. Res. Lett.*, *31*, L14604, doi:10.1029/2004GL020020.

Johnson, J. B., J. M. Lees, A. Gerst, D. Sahagian, and N. Varley (2008), Long-period earthquakes and co-eruptive dome inflation see with particle image velocimetry, *Nature*, *456*, 377–381, doi:10.1038/nature07429.

Jones, K. R., and J. B. Johnson (2010), Mapping complex eruptive activity at Santiaguito, Guatemala using network infrasound semblance, *J. Volcanol. Geotherm. Res.*, doi:10.1016/j.jvolgeores.2010.08.006, in press.

Kinney, G. F., and K. J. Graham (1985), *Explosive Shocks in Air*, 269 pp., Springer, New York.

Lyons, J. J., G. P. Waite, W. I. Rose, and G. Chigna (2010), Patterns in open vent, strombolian behavior at Fuego volcano, Guatemala, 2005–2007, *Bull. Volcanol.*, *72*(1), 1–15, doi:10.1007/s00445-009-0305-7.

Marchetti, E., M. Ripepe, A. J. L. Harris, and D. Delle Donne (2009), Tracing the differences between Vulcanian and Strombolian explosions using infrasonic and thermal radiation energy, *Earth Planet. Sci. Lett.*, *279*(3–4), 273–281, doi:10.1016/j.epsl.2009.01.004.

Morrissey, M. M., and B. A. Chouet (1997), Burst conditions of explosive volcanic eruptions recorded on microbaragraphs, *Science*, *275*(5304), 1290–1293, doi:10.1126/science.275.5304.1290.

Ripepe, M., M. Coltelli, E. Privitera, S. Gresta, M. Moretti, and D. Piccinini (2001), Seismic and infrasonic evidences for an impulsive source of the shallow volcanic tremor at Mt. Etna, Italy, *Geophys. Res. Lett.*, *28*(6), 1071–1074, doi:10.1029/2000GL011391.

Rowe, C. A., R. C. Aster, P. R. Kyle, R. R. Dibble, and J. W. Schlue (2000), Seismic and acoustic observations at Mount Erebus Volcano, Ross Island, Antarctica, 1994–1998, *J. Volcanol. Geotherm. Res.*, *101*(1–2), 105–128, doi:10.1016/S0377-0273(00)00170-0.

Ruiz, M. C., J. M. Lees, and J. B. Johnson (2005), Source constraints of Tungurahua volcano explosion events, *Bull. Volcanol.*, *68*, 480–490, doi:10.1007/s00445-00005-00023-00448.

Yamamoto, H., I. M. Watson, J. C. Phillips, and G. C. Bluth (2008), Rise dynamics and relative ash distribution in vulcanian eruption plumes at Santiaguito Volcano, Guatemala, revealed using an ultraviolet imaging camera, *Geophys. Res. Lett.*, *35*, L08314, doi:10.1029/2007GL032008.

Yokoo, A., T. Tameguri, and M. Iguchi (2009), Swelling of a lava plug associated with a Vulcanian eruption at Sakurajima Volcano, Japan, as revealed by infrasound record: Case study of the eruption on January 2, 2007, *Bull. Volcanol.*, *71*(6), 619–630, doi:10.1007/s00445-008-0247-5.

J. B. Johnson, Department of Earth and Environmental Science, New Mexico Institute of Mining and Technology, Socorro, NM 87801, USA.

J. M. Lees, Department of Geological Sciences, University of North Carolina, Chapel Hill, NC 27599, USA.